TAO, Vol.5, No.4, 537-555, December 1994

# Cloud Influence on Microwave Sensing of the Ocean

LEONID MITNIK[1,2], MING-KUANG HSU[1], CHO-TENG LIU[3] and MAYA MITNIK[2]

(Manuscript received 7 July 1994, in final form 16 November 1994)

## ABSTRACT

**The usage of satellite IR (infrared) and visible techniques to study oceanographic phenomena and processes in the waters surrounding Taiwan presents serious difficulties because of cloudiness and fogs. The usage of microwave sensors, however, allows this difficulty to be overcome since cloud is a semi-transparent medium for microwaves. The main factors influencing the atmospheric microwave emission and attenuation are molecular oxygen, water vapor, clouds and precipitation. Dependencies of microwave absorption due to small cloud droplets and ice particles on wavelength and temperature are given in other papers. Based on microwave measurements of atmosphere emission, the technique for estimating the total cloud absorption and the total cloud liquid water content is described. Experimental data on cloud and rain emission at wavelengths of 2.3 cm were obtained near the northern coast of Taiwan. Detailed analyses of the microwave measurements of different kinds of cloudiness and rains together with weather maps, satellite infrared images, radiosonde data and rain gauge data covering February 19 and March 19-20, 1994 are presented. These microwave measurements are used in this paper to estimate the typical spatial scales of total cloud absorption variations, a distribution of cloudiness in the total (integrated) liquid water content and the influence of winter monsoon clouds near Taiwan on ocean sensing at frequencies of the Special Sensor Microwave/Imager. The probability of heavy clouds with a total liquid water content 1 kg/m$^2$ significantly influencing on satellite microwave sensing of the ocean, was about 2.5%.**

**(Key words: Microwave measurements, Cloud absorption, Total cloud liquid water content, Rain, SSM/I, Microwave ocean sensing, Winter monsoon)**

## 1. INTRODUCTION

In accordance with climatic data (Climatic Atlas of Taiwan, 1991) the probability of clear sky on most of the coastal and island stations (Pengchiayu, Tanshui, Keelung, Hualien,

[1] Department of Oceanography, National Taiwan Ocean University, Keelung, Taiwan, R.O.C.

[2] Pacific Oceanological Institute, Russian Academy of Sciences, Vladivostok, Russia

[3] Institute of Oceanography, National Taiwan University, Taipei, Taiwan, R.O.C.

Tungchitao, Chengkung, Taitung, Tawu, Lanyu) is, as a rule, below 10% year round and only reaches 11-13% on some stations (Keelung, Tungchitao) during the summer period. The probability of days with scattered-clouds (when the volume of clouds reaches 1 to 6) may be as high as 30-45% on a number of stations during several months. The number of fog days is, as a rule, low. However, the mean fog days in Keelung and to the north of Taiwan (Pengchiayu) reaches 4-6 in March-June. These estimates of cloudiness and fog are typical in all areas around Taiwan. The probability of days with a cloud volume between 0 and 3 is 10%-20% in August and 20%-30% in February, May and November. The average total cloud volume is equal to 6-7 in November-April and June, and 5-6 in May and July-October (Pacific Ocean, 1974). Cloudy and cloudless days distribute non-uniformly over the year. Sometimes during winter monsoon and Mei-Yu periods, continuous cloudiness and precipitation are observed up to 30-60 days. As a result, in spite of daily observations during more than 10 years, only a limited quantity of satellite IR images showing Kuroshio features and the upwelling area north of Taiwan has been gathered.

As one example, Figure 1 shows the rare occasion of a nearly cloud free satellite thermal image around Taiwan and the sea east of it. In Figure 1a of the thermal image of the surrounding waters of Taiwan on January 17 of 1994, it is easy to see the warm (reddish color) Kuroshio flowing past the east of Taiwan with its warm branch in the Taiwan Strait, and a warm pool southwest of Taiwan. The cold pool north of Taiwan may be the result of local upwelling. About twelve hours later, most of Taiwan and the sea north of it was covered by cloud (Figure 1b). This is to say that for a synoptic scale study, one has little chance (about 3% it is estimated) to have an IR image with a large cloud-free area. To have contiguous cloud-free images from the East China Sea to the Luzon Islands for more than one day, the chances are even lower (1% according to these authors experience). Without continuous satellite coverage as caused by cloud, studies on the possible periodicity of upwelling, surface currents, and the interaction of the Kuroshio with coastal fronts, etc. are certainly hampered.

A high probability of cloudiness is typical of many other regions where information on sea surface properties is important in solving practical and scientific problems.. Attenuation due to clouds and precipitation, is significantly less for microwave than for visible and infrared radiation. Usage of microwave sensors allows to overcome this difficulty because cloud is a semitransparent medium for microwaves. This factor, in combination with the additional possibilities of influences from the environmental parameters have led to a significant increase in the number of different satelliteborne microwave systems in recent years. These include the Special Sensor Microwave/Imager (SSM/I), TOPEX/POSEIDON altimeter and microwave radiometers, the Okean Real Aperture Radar (RAR), ERS-1 Synthetic Aperture Radar (SAR) and microwave radiometers. Several other systems are scheduled to be launched in the coming years, like the Ikar Microwave Complex of the Priroda module (Russia), TRMM (USA-Japan) and RADARSAT (Canada), etc..

Results of satellite microwave sensing allow for the estimation of the sea surface temperature (SST), surface wind velocity, and the integrated atmospheric parameters: the total water vapor content $V$ (precipitable water) and the total (integrated) cloud liquid water content $Q$. These estimates, in turn, may be used to correct infrared estimates of SST (Emery *et al.*, 1994), and to calculate the surface-level humidity (Liu, 1986), the pressure (Brown and Levy, 1986), as well as the fluxes of latent and sensible heat at the ocean-atmosphere boundary (Grankov, 1992; Liu, 1988), etc..

Errors from the satellite-derived oceanic parameters depend on atmospheric emission and attenuation. The main factors influencing on the atmospheric microwave emission and

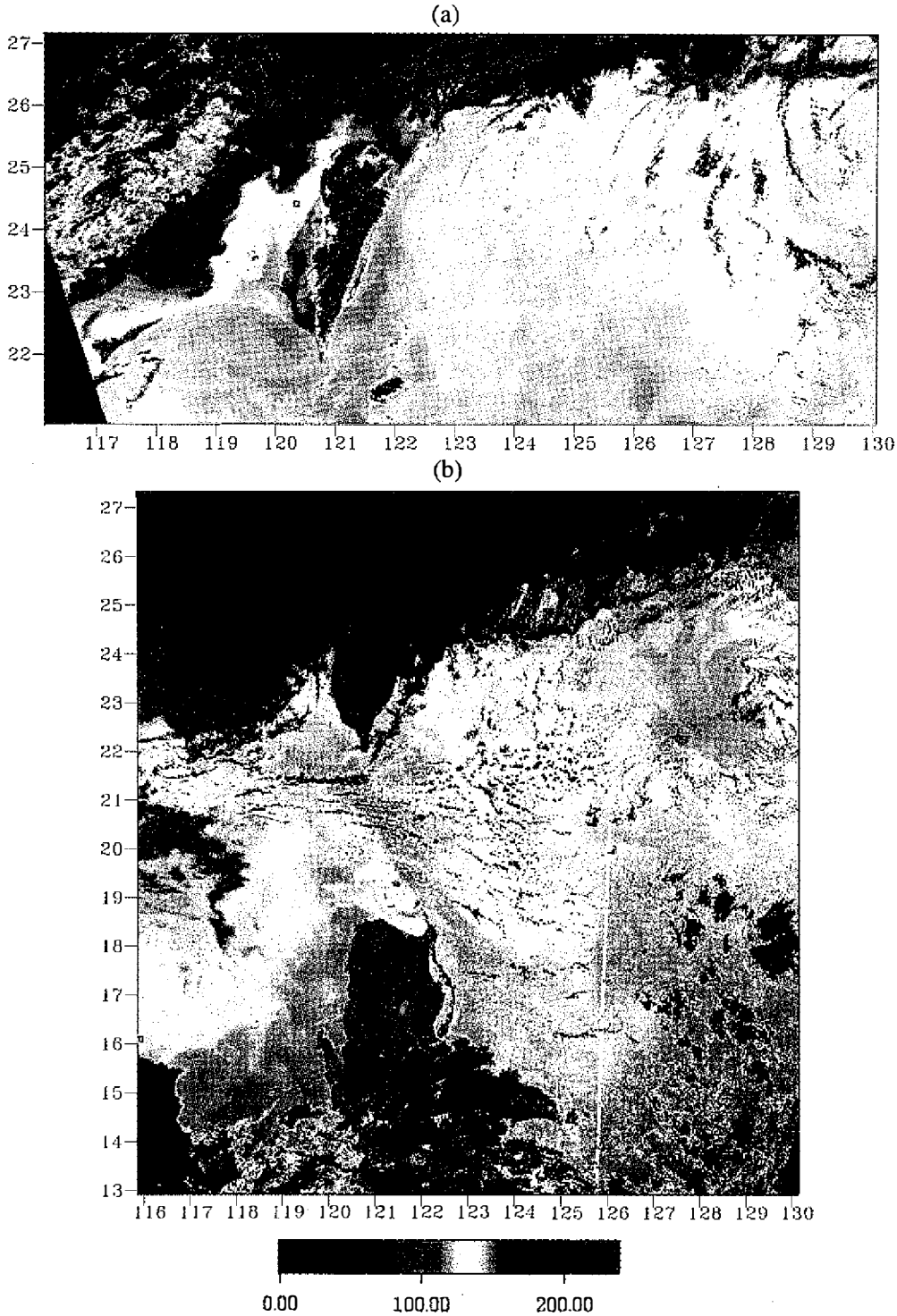


*Fig. 1.* Satellite thermal images over the Taiwan area on January 17, 1994. (a) afternoon image, (b) next morning image. The spatial scale is 1.1 km for each pixel, and the number of pixels of each image is indicated as the label of axes.

attenuation are molecular oxygen, water vapor, clouds and precipitation. Total absorption due to oxygen, $\Gamma_{ox}$, does not exceed 0.1 neper at frequencies below 40 GHz and over the range of 80-110 GHz. Its variation can be accurately calculated using surface air temperature and pressure data. To the first order approximation, the total absorption due to water vapor, $\Gamma_{vw}$, is proportional to $V$. At frequencies $f < 15$ GHz, $\Gamma_{vw}$ is small and negligible in most cases. Near the resonance frequencies of water vapor, e.g. at $f = 22.235$ GHz and at $f >$ 70 GHz, $\Gamma_{vw}$ exceeds 0.2 neper for a typical tropical atmosphere having $V > 40$ kg/m$^2$.

The total absorption due to cloud, $\Gamma_{cl}$, depends on the liquid water content and the temperature of cloud. The cloud absorption increases with frequency and with the decrease in the cloud droplet temperature. $\Gamma_{cl}$ changes over a wide range as a function of cloud type. Spatial variations of $Q$, and hence $\Gamma_{cl}$, are large for convective forms of clouds and significantly less for strati forms. From the above discussions, a need for a comprehensive consideration of the possible limitations of remote sensing of the oceans by microwaves at cloud conditions is obvious.

A large body of data on total cloud liquid water content was obtained from satellite microwave measurements with spatial resolution ranging from several hundreds to several thousands of square kilometers. The ground and airborne measurements could provide data with a much higher resolution needed to study the fine structure of $Q$ and to estimate the influence of clouds on both active (SAR, RAR, altimeter, scatterometer) and passive sensors. To investigate the microwave properties of cloud and rain in the Taiwan region, a radiometer operating at $f = 13.1$ GHz was used. At this frequency, the main source of signal variability is the change in the total liquid water content in the atmosphere. Knowledge of the regional features of atmospheric emission and attenuation can be used to improve the accuracy of the SST, surface wind speed, water vapor, liquid water content and the rain rate retrieval algorithms that have global character (Bauer and Schluessel, 1993; Goodberlet and Swift, 1992; Schulz *et al.*, 1993; Wentz, 1992).

The main goals of this paper are to consider the features of the absorption spectrum due to clouds, to describe results of ground-based cloud emission measurements at the wavelength of 2.3 cm and to estimate the influence of cloud absorption on space measurements at other wavelengths..

## 2. ABSORPTION AND SCATTERING OF MICROWAVES IN CLOUDS

### 2.1 Water Clouds

The interaction of microwave radiation with cloud droplets is determined by the normalized size parameter, $a_\lambda = 2\pi r/\lambda$, the ratio of the circumference $2\pi r$ of a spherical particle to the wavelength $\lambda$ of the incident radiation. In the general case, it is necessary to take into account both absorption and scattering. The relationships for the attenuation, scattering and absorption cross sections that are normalized with the parameter $\pi r^2$ represent Mie sets. The terms of these sets contain Bessel and Hankel functions from arguments of $a_\lambda$ and the complex index of the refraction of particles (Shifrin, 1951; Van de Hulst, 1957).

When the condition $a_\lambda \leq 0.7$ holds (Platt, 1970), an approximate relationship can be written for the attenuation section (Shifrin, 1951; Van de Hulst, 1957):

$$Q_{att} = Q_{abs} + Q_{scat} = -\mathrm{Im}\left(4a_\lambda\alpha + \tfrac{4}{15}a_\lambda^3\alpha\tfrac{\varepsilon^2+27\varepsilon+38}{2\varepsilon+3}\right) + \frac{4}{3}a_\lambda^4\,\mathrm{Re}(\alpha^2) \qquad (1)$$

where $\varepsilon = \varepsilon' - i\varepsilon''$ is the complex dielectric permittivity of water, which is a function of wavelength and temperature, $\alpha = (\varepsilon\text{-}1)/(\varepsilon+2)$. Im and Re designate the imaginary and real parts, respectively.

If droplet sizes satisfy the stronger condition $a_\lambda \leq 0.2$ (or $r < 0.1\lambda/\pi$), scattering can be neglected and Equation (1) may be simplified as:

$$Q_{att} = Q_{abs} = -4a_\lambda \, \mathrm{Im}(\alpha).$$

To calculate coefficients of the attenuation of the plane electromagnetic wave ($\gamma_{att}$) in its passage through a cloud layer, it is necessary to sum the attenuation values over all droplets:

$$\gamma_{att} = \int_{r_1}^{r_2} \pi r^2 n(r) Q_{att}[\lambda, n(r)] dr,$$

where $n(r)$ is droplet size distribution function, while $r_1$ and $r_2$ are the smallest and the largest radii of droplets respectively.

If the inequality $a_\lambda \leq 0.2$ holds for all droplets at a given wavelength, then the variations of the function of $n(r)$ has no influence on attenuation, and $\gamma_{att}$ is proportional to the liquid water content of cloud $w$ (in g/m$^3$)

$$\gamma_{att} = \gamma_{abs} = -\frac{6\pi V_d}{\lambda}\mathrm{Im}(\alpha) = -\frac{6\pi w}{\lambda\rho}\mathrm{Im}(\alpha),$$

where $V_d = \frac{4}{3}\pi \int_{r_1}^{r_2} r^3 n(r) dr$ is the droplet volume, and $\rho$ is the droplet density.

After calculating the imaginary part of $\alpha$ and substituting the wavelength $\lambda$ with frequency $f$, the cloud absorption coefficient $\Gamma_{cl}$ may be derived as a product of the mass absorption coefficient and the liquid water content $w$:

$$\gamma_{cl} = 0.06\pi f \frac{\varepsilon''(f)}{[\varepsilon'(f)+2]^2 + [\varepsilon''(f)]^2} w \qquad (2)$$

where $f$ is frequency in GHz.

At $f < 100$ GHz, a small-particle approximation holds for almost all clouds (Deirmendjian, 1975). Pruppacher (1981) showed a representative droplet size spectra for a variety of non-precipitating clouds, both continental and maritime. With a few exceptions, the number concentration $n(r)$ of droplets with the radius $r > 30$ $\mu$m is quite small. Further calculations prove that the fractional contribution to the total cloud liquid water content by these larger droplets is also small.

Figure 2 demonstrates the mass absorption spectra due to cloud for the droplet temperatures $t_{cl}$= -20°C, 0°C and 20°C. According to the formulae given by Rosenberg (1972), the dielectric permittivity of water droplets may be calculated as a function of frequency and temperature (including super-cooled droplets). Unusual features of the microwave cloud absorption spectrum resides in the fact that a decrease in $t_{cl}$ is accompanied by a significant increase in absorption. As a result, the emission of an optically thin cloud at $f < 70$ GHz increases with a decrease in its thermodynamic temperature (Shifrin and Chernyak, 1974; Petty and Katsaros, 1992).

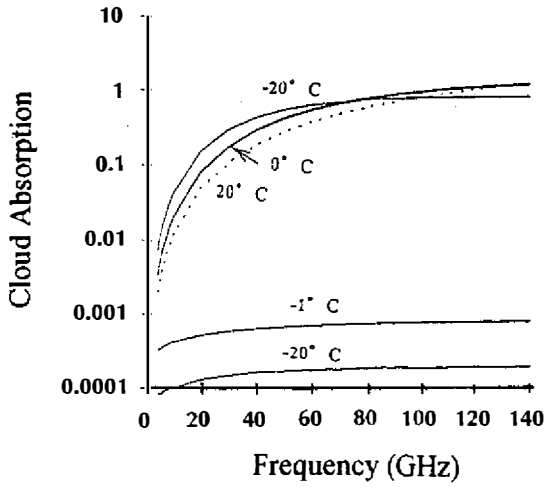


*Fig. 2.* The spectra of mass absorption coefficients for water clouds with temperatures: 20°C, 0°C, and -20°C and ice clouds with temperatures: -1°C and -20°C.

At air temperature $t \leq 0°C$, the water in clouds is in both the liquid phase (water or droplet clouds) and the solid phase (ice or crystal clouds). Super-cooled droplets are often observed in upper and middle layer clouds and in the upper part of heavy clouds such as cumulus congestus. The liquid phase of water is often observed at $t \leq$ -10°C, and it is detected even at $t$ = -40°C. There are no measurements of the dielectric permittivity of water at such low negative temperatures and, thus, values of $\varepsilon$ are calculated by extrapolation of the same formulae as for positive temperatures (Rosenberg, 1972). This factor may cause additional errors (Mitnik, 1984).

### 2.2 Ice Clouds

The appearance of the solid (ice) phase of water in cloud increases with the decrease in temperature. The dielectric characteristics of ice differs sharply from those of water. The real part of $\varepsilon$ is about 3.15, and it depends weakly on the frequency and the temperature. The imaginary part of $\varepsilon$ is considerably less than that of water, and it decreases sharply with the decrease in temperature and with the increase in frequency (Liebe *et al.*, 1989). Using data from Ray (1972) and Equation (2), Mitnik (1979) obtained the following relationship for ice cloud absorption:

$$\gamma_{cl}(f,t) \approx 2.2 \cdot 10^{-4} f^{1/3}(1 + 0.095t_{cl} + 0.0028t_{cl}^2)w.$$

The mass absorption coefficient of an ice cloud is more than two-to-three orders of magnitude lower than that of a water cloud (see curves 4 and 5 in Figure 2). Because the total ice content in most clouds is much less than 0.1 kg/m$^2$, its contribution of $\Gamma_{cl}$ to the measured brightness temperature is negligible for both the ice clouds and the ice component of mixed-phased clouds.

### 2.3 Approximation Equations for Water Clouds

Several approximation equations for cloud absorption which do not require calculations of the dielectric permittivity of water were suggested (Staelin, 1966; Chernyak, 1970; Petty and Katsaros, 1992). Staelin (1966) obtained a formula for $f < 50$ GHz:

$$\gamma_{cl}(f, t_{cl}) = 1.11 \cdot 10^{[0.0122(291 - t_{cl} - 4]} f^2 w,$$

where $t_{cl}$ is the cloud temperature in °K. Chernyak (1970) tabulated the dependence on cloud temperature $t_{cl}$ (in °C) for different wavelengths $\lambda$ *via* the coefficient B($\lambda, t_{cl}$):

$$\gamma_{cl}(\lambda, t) = B(\lambda, t_{cl}) \frac{0.112}{\lambda^2 + 0.0269} w.$$

Values of $B(\lambda, t_{cl})$ for several wavelengths are given in Table 1.

Table 1. List of coefficients $B(\lambda, t_{cl})$ normalized at $t_{cl}$ = 20°C.

| Wavelength | Frequency | Temperature (°C) | | | | |
|---|---|---|---|---|---|---|
| (cm) | (GHz) | -10 | 0 | 10 | 20 | 30 |
| 0.5 | 60.0 | 1.69 | 1.45 | 1.20 | 1 | 0.84 |
| 0.6 | 50.0 | 1.87 | 1.53 | 1.22 | 1 | 0.83 |
| 0.8 | 37.5 | 2.11 | 1.59 | 1.23 | 1 | 0.83 |
| 1.35 | 22.2 | 2.39 | 1.68 | 1.27 | 1 | 0.813 |
| 1.6 | 18.8 | 2.31 | 1.67 | 1.29 | 1 | 0.805 |
| 3.2 | 9.4 | 2.51 | 1.70 | 1.27 | 1 | 0.805 |

Since 1987, continuous microwave sensing of the Earth has been carried out by the SSM/I on board the satellites of the United States Defense Meteorological Satellite Program (DMSP) (Hollinger, 1989). Seven channels of the SSM/I sense atmospheric and surface thermal emission at 19.35, 22.235, 37.0 and 85.5 GHz. Petty and Katsaros (1992) used a separate fit of $\gamma_{cl}$ to temperature for the interval -20°C to 35°C for each SSM/I frequency. A complex permittivity of water was calculated from the Liebe *et al.* (1991) model. Table 2 gives the following coefficients $C_i$ for a fit of $\gamma_{cl}$ to $t_{cl}$ (°C):

$$\gamma_{cl} \approx \exp[C_o + C_1 t_{cl} + C_2 t_{cl}^2 + C_3 t_{cl}^3].$$

Table 2. Coefficients $C_i$ for the SSM/I frequencies.

| Frequency (GHz) | $C_0$ | $C_1$ | $C_2$ | $C_3$ | Maximum error (%) |
|---|---|---|---|---|---|
| 19.35 | -2.55 | -0.0298 | $0.681 \times 10^{-4}$ | $0.335 \times 10^{-5}$ | 1.6 |
| 22.235 | -2.28 | -0.0289 | $0.346 \times 10^{-4}$ | $0.381 \times 10^{-5}$ | 1.2 |
| 37.0 | -1.35 | -0.0234 | $-0.122 \times 10^{-3}$ | $0.548 \times 10^{-5}$ | 1.4 |
| 85.5 | -0.0713 | $-0.800 \times 10^{-2}$ | $-0.162 \times 10^{-3}$ | $0.118 \times 10^{-5}$ | 1.0 |

## 3. INSTRUMENT DESCRIPTION

Microwave measurements of cloud and rain emissions were performed with a Dicke modulation radiometer operating at frequency $f$ = 13.1 GHz with 1 GHz bandwidth and about 0.2°K sensitivity at 1 s time constant. The radiometer was made in the Chita Institute of Natural Resources, Siberian Branch of the Russian Academy of Sciences. It consists of a microwave unit and a low-frequency (control) unit that are connected with a 10-m cable. This radiometer was calibrated by an internal semiconductor noise generator and also by a comparison of emission levels of matched load and cloudless sky. The matched load (attenuator) was inside the microwave unit near the radiometer input. Its temperature was measured by a thermocouple. The atmospheric emission was collected by a horn-lens antenna with a beamwidth of 6.3°. The results of the measurements were recorded with a paper recorder in analog form and on a personal computer after digitization (Figure 3a).

The radiometer was installed in the Department of Oceanography, National Taiwan Ocean University (Figure 3b). The microwave and control units were kept indoors and maintained at room temperature to minimize the influence of changing weather conditions. After the warm-up period, the internal temperature variation was under 1°K. The microwave unit was mounted on a frame with adjustable elevation. A microwave-transparent film was used to replace the glass window. The canopy protected the film from any rain droplets which could have distorted the measurements. This setup worked well except during strong northeasterly winds when a varying force may exert directly on the film. A comparison of the signal levels received with and without the droplets on the film showed that, at $\lambda$ = 2.3 cm, the interference (emission and absorption) from the droplets was small in most cases. The researchers were able to use a ventilator to blow away the rain droplets and also to dry out the film. This is generally critical for measurements at shorter wavelengths (Demoz *et al.*, 1993).

## 4. METHODS OF MEASUREMENTS

Observations of the cloud and rain emissions were carried out at zenith angles $\beta \leq 70°$ (Figure 3a). They are parameterized with the increments, $\Delta T_B(\beta)$, in the brightness temperatures of the cloudy areas, $T_B^{cl}(\beta)$, against the cloud-free (clear) background, $T_B^{\circ}(\beta)$:

$$\Delta T_B(\beta) = T_B^{cl}(\beta) - T_B^{\circ}(\beta).$$

For simplicity, the atmosphere is assumed to be horizontally uniform and the effective temperatures of the cloudy and the clear atmospheres are equal. At $\lambda$ = 2.3 cm, the condition $a\lambda \leq 0.2$ holds for those droplets with $r < 0.73$ mm. This covers all forms of clouds, drizzles, weak and moderate rains (with intensity below 5-6 mm/h). The assumption that the scattering is negligible for all water droplets (Mitnik *et al.*, 1993) produces:

$$\Delta T_B(\beta) = T_{eff}\exp(-\Gamma_{\circ}\sec\beta)[1 - \exp(-\Gamma_{cl}\sec\beta)], \quad (3)$$

where $T_{eff} = T_{\circ} - \Delta T$, $T_{\circ}$ is the air temperature at the level of radiometer installation, and $\Delta T$ (about 10°K~20°K) is a correction for the non-isothermity of the atmosphere. This depends on the vertical profiles of the air temperature and atmospheric absorption, $\Gamma_{\circ}$ is the

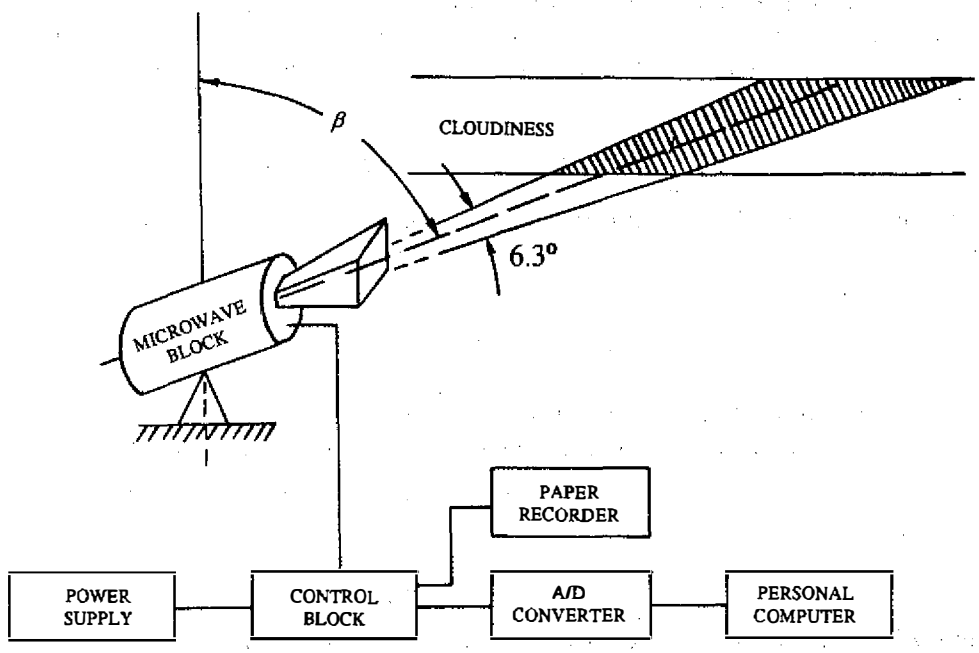


(a)

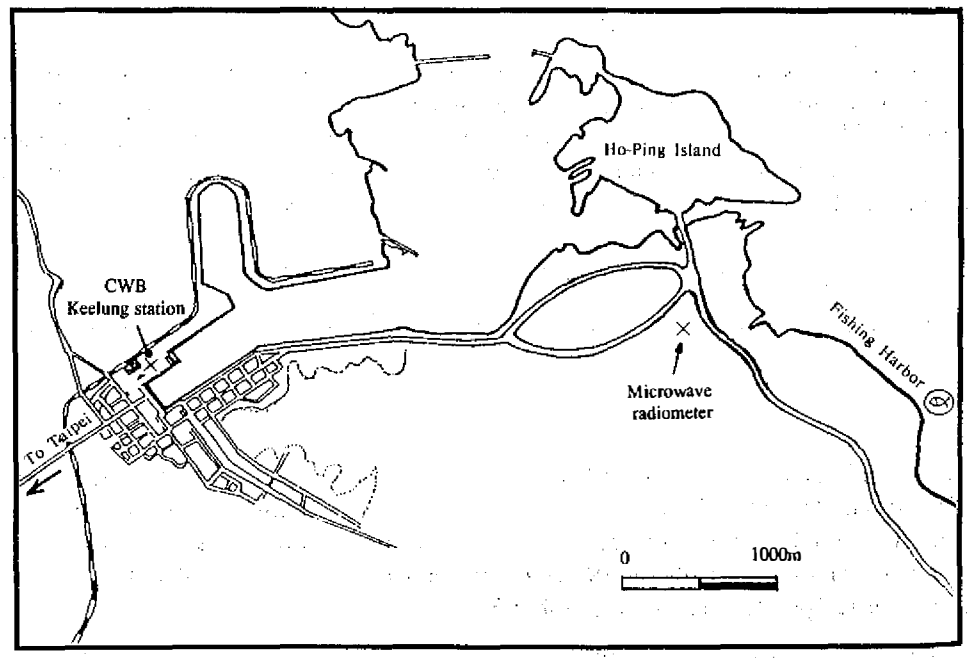


(b)

*Fig. 3.* (a) Diagram of measurements of microwave atmospheric emission; (b) Locations of the microwave radiometer and the rain gauge.

total absorption of the cloud-free atmosphere (a sum of absorptions due to oxygen $\Gamma_{ox} \approx 0.013$ and due to water vapor $\Gamma_{vw} \approx 0.00037V$), while $\Gamma_{cl}$ is the total absorption of the cloudy atmosphere minus $\Gamma_o$. $\Gamma_o$ is small and is assumed to be known. It follows from Equation (3) that

$$\Gamma_{cl} = -(1/\sec\beta)\ln\{1 - [\Delta T_B(\beta)/T_{eff}]\exp(\Gamma_o \sec\beta)\}. \quad (4)$$

$\Gamma_{cl}$ is determined by the vertical profiles of liquid water content and temperature in the cloud

$$\Gamma_{cl} = \int_o^l \gamma_{cl}[t(l)]w(l)dl, \quad (5)$$

where $l$ is the path length of the microwave radiation in a cloud.

In an isothermal cloud, $t(l)$ is constant and $\Gamma_{cl}$ is proportional to the total cloud liquid water content $Q = \int_o^l w(l)dl$. For a non-isothermal cloud, $t(l) \neq$ constant, and Equation (5) may be written as

$$\Gamma_{cl} = \gamma_{cl}(t_{cl})Q \quad (6)$$

where $t_{cl}$ is the effective cloud temperature which is determined from the condition where

$$\gamma_{cl}(t_{cl}) = \int_o^l \gamma_{cl}[t(l)]w(l)dl / \int_o^l w(l)dl.$$

For rains with small droplets, the value of $Q$ in (6) represents the sum of the total liquid water content in cloud and precipitation. (For rains with large droplets, a rough estimation of rain intensity $R$ can be derived from Equation (4) if $Q$ is given. A special consideration is required to estimate errors originating in the process). For a small increase in the brightness temperature, $\Delta T_B$, Equation (4) can be simplified using ln(1-x) $\approx$ x:

$$\Gamma_{cl} \approx (1/\sec\beta)\Delta T_B(\beta)\exp(\Gamma_o \sec\beta)/T_{eff} \quad (7)$$

For zenith angle $\beta$=69°, $T_{eff}$ = 280°K, and $V$ = 45 kg/m$^2$, $\Gamma_{cl}$ may be approximated as:

$$\Gamma_{cl} \approx 0.00132\Delta T_B.$$

The error of this expression is about 2% if $\Delta T_B \leq 13$°K or about 5% if $\Delta T_B \leq 26$°K.

To estimate the total cloud liquid water content from relationship (6), it is necessary to know the function $\Gamma_{cl}$ ($t_{cl}$) and specify $t_{cl}$. Based on Equation (2) and the dielectric permittivity of water from Rosenberg (1972), the dependence of the cloud absorption coefficient on the droplet temperature is listed in Table 3.

Table 3. Cloud mass absorption coefficient $\gamma_{cl}$ at $f$ = 13.1 GHz as a function of temperature.

| Temperature,(°C) | -30 | -20 | -10 | 0 | 10 | 20 | 30 |
|---|---|---|---|---|---|---|---|
| Absorption, neper/(kg/m$^2$) | 0.106 | 0.0723 | 0.0504 | 0.0361 | 0.0271 | 0.0213 | 0.0173 |

The total cloud liquid water content may be determined by Equations (4) or (7), and Equation (6) at the given cloud temperature. In particular, the values of $Q$ corresponding to the $\Delta T_B \approx 13°K$ - $26°K$ are about 0.6 kg/m$^2$ - 1.2 kg/m$^2$ assuming that $t_{cl}$ =10°C. This covers the majority of the observed forms of cloudiness. From the above, it follows that the $\Delta T_B$ profile represents essentially the $Q$ profile at a definite scale if the possible changes of $t_{cl}$ are neglected. The $Q$ scale is practically linear at $\Delta T_B < 25°K$-$30°K$. Nonlinearity increases with $\Delta T_B$.

Ambiguity in the cloud temperature is the main source of error in estimating $Q$ from $\Gamma_{cl}$. As seen from Table 3, if the given $t_{cl}$ differs from the true $t_{cl}$ by $\pm 10°C$, then the relative errors in $Q$ are -22% and +33% in the case of $t_{cl}$ = 10°C.

## 5. EXPERIMENTAL RESULTS

The measurements of cloud emission were started on December 28, 1993. The antenna was directed northeastward, against the prevailing winds during the winter monsoon. The measured brightness temperatures are volume-averaged values. The averaged volume depends on the antenna beamwidth and viewing angle, and the heights of the lower and upper boundaries of the cloud layer (Figure 3a). The duration of the continuous measurements of the atmospheric emission changed from several hours to over a week, depending on the duration of cloudiness over Keelung. The antenna was directed northeastly, against the prevailing winds during winter monsoon.

Most of the time, stratus (St), strato-cumulus (Sc) and nimbo-stratus (Ns) clouds with little rain (drizzle) or without rain were observed. An appearance of stratus forms of cloudiness was also supported by analysis of On the IR satellite images, where these clouds were presented in a gray tone. At these forms of cloudiness tThe average values of the brightness temperature increments for these forms of cloudiness were usually below 6°K-10°K. From this and Equations (6) and (8), it follows that the total cloud liquid water content in zenith was below 0.3 kg/m$^2$ - 0.45 kg/m$^2$ at $t_{cl}$ = 10°C-15°C. Without precipitation, the variations of $T_B$ were slow and small. These variations increased during rain and when individual cumulus cloud drifted into the antenna beam.

In comparison with stratiform clouds, the passage of cumulus (Cu) and nimbus (Nb) clouds were usually accompanied by larger mean values and increased temporal (spatial) variations of $T_B$. The intensity of rain was higher too. These clouds are expressed in a brighter tone on the satellite IR images showing their low cloud top temperature.

With these general notes discussed, the time variations in the brightness temperature of the atmosphere observed north of Taiwan are considered.

**Case 1.** On February 19, 1994, a cloud system covered the whole Taiwan area, including the sea surrounding it. The system was associated with a non-deep cyclone which moved eastward slowly on a series of GMS-4 IR images provided by the Central Weather Bureau (CWB). The NNW-NW surface wind speed at Pengchiayu island was 7 m/s at 1100 and 1500 LST (local standard time) of February 19. Alternating gray and dark-gray bands are distinguishable on the satellite images. Displacement of the considered cloud system was sometimes accompanied by significant variations in the brightness temperature (see a fragment of measurements in Figure 4). The arrows on the horizontal axis in Figure 4 show the times when the GMS-4 images were taken. The increments of $\Delta T_B$ increased significantly at 1020-1030 LST and between 1215 and 1500 LST when drizzle and rain were observed.

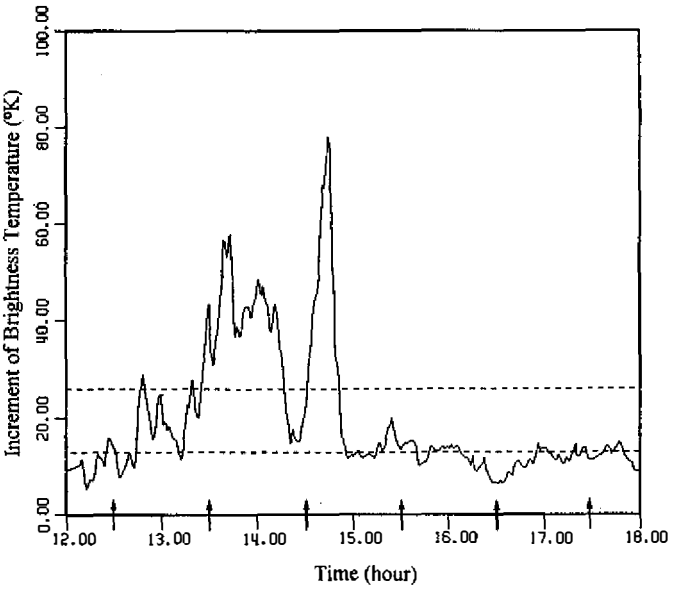


*Fig. 4.* The brightness temperature increment of cloudy atmosphere $\Delta T_B$ relative to the level of clear sky emission taken at the wavelength of 2.3 cm in Keelung on February 19, 1994.

The total water vapor content of the atmosphere calculated from aerological data near Taiwan at 0800 LST was rather quite high, $V \approx 46.5$ kg/m$^2$.

The values of the total cloud liquid water content should be noted. The two lines parallel to the time axis in Figure 4 show the increments of $\Delta T_B$ = 13°K and 26°K corresponding to $Q$ = 0.6 kg/m$^2$ and 1.2 kg/m$^2$ (at $t_{cl}$ = 10°C), respectively. When $\Delta T_B$ > 26°K, the approximated Equation (7) gives underestimated values of $\Gamma_{cl}$ (and hence $Q$) and Equation (4) should be used. For example, at $\Delta T_B$ = 40°K, $\Gamma_{cl}$ = 0.0605 ($Q$ = 2.23 kg/m$^2$ at $t_{cl}$ = 10°C). The largest $\Delta T_B$ were observed between 1310 and 1450 LST (with a 15 min. gap after 1410 LST) when the rain rate increased, especially at about 1435-1450 LST. A convective rain cell may have crossed the antenna beam at this time. The slope of the brightness temperature versus the time reached about 7°K/min during the passing of the rain cell.

During the following 32 h, stratiform clouds passed over the Keelung area. The $T_B$ varied slowly and smoothly as seen in the right portion of Figure 4. The values of $\Delta T_B$ exceeded 26°K (not shown in Figure 4) but only during three 5-min intervals.

**Case 2.** On March 12-26, 1994, the measurements were nearly uninterrupted. The temperature inside the microwave unit and the level of the calibration signal were practically constant. Figure 5 shows the fragment of measurements taken between 0900 LST on March 19 and 0900 LST on March 20. According to the weather maps prepared by the CWB, the atmospheric front crossed central Taiwan. The total water vapor content of the atmosphere V was high. Aerological data taken near Taipei at 2000 LST March 18 reported $V \approx 48$ kg/m$^2$. Rain of different intensities as well as drizzle were observed. From a series of GMS-4 IR images provided by CWB, a dense cloud system with a relatively high upper boundary was located northwest of Taiwan in the morning of March 19. The cloudiness over Taiwan was

not so dense and heavy. The system shifted to the east and its southern part crossed northern and central Taiwan. The meteorological station on Pengchiayu island reported a NE-NNE wind speed of 10 m/s at 1100 and 1700 LST on March 19. The arrows in Figure 5 note the times when the GMS images were taken. One of the GMS images is shown in Figure 6. The tone of the cloudiness was homogeneous, probably because of cirri.

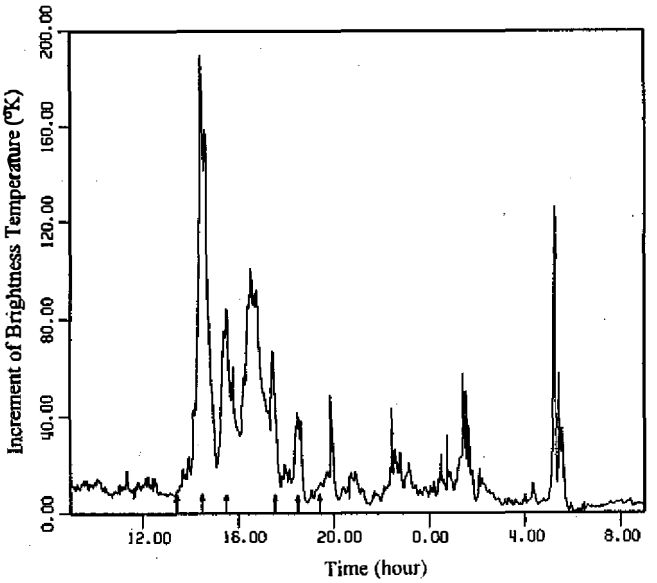


*Fig. 5.* The same as in Figure 4 but on March 19-20, 1994.

The lowest values of $\Delta T_B$ at low-magnitude and slow time variations were observed between 0220 and 0500 and after 0550 LST on March 20 (Figure 5). The values of $Q$ were 0.1-0.4 kg/m$^2$ (assuming that $t_{cl}$ = 10-15°C) which is typical for stratus form clouds. Before 1400 LST on March 19 and between 2300 on March 19 and 0100 LST on March 20, the $\Delta T_B$ values were somewhat larger, and the $\Delta T_B$ profile was sometimes highly jagged. The values of the total liquid water content of the atmosphere (cloud and rain - mainly drizzle) ranged between 0.3 and 1.0 kg/m$^2$.

$\Delta T_B$ increased significantly (Figure 5) while the cloud system (Figure 6) was crossing northern Taiwan. Several peaks of $\Delta T_B$ were distinct, and they lasted for a few ten-minute intervals. The magnitude of the first one was the largest and reached 190°K. Strong rain was observed at that time. Because the number of large droplets increased with the rain rate, the condition $a\lambda \leq 0.2$ is invalid. During the rain, the value of total absorption calculated by Equation (4) is essentially the approximate total absorption due to liquid water in the atmosphere, $\Gamma_l$. This represents the sum of cloud and rain absorption $\Gamma_l = \Gamma_{cl} + \Gamma_r$.

Since the microwave emission under heavy rain needs special consideration (Kummerov and Weinman, 1988) and is beyond the scope of this research, the authors only comment on it a little. The rain rate may be estimated by the relationship

$$\Gamma_r = \Gamma_l - \gamma_{cl}(t_{cl})Q = L\,\gamma_r,$$

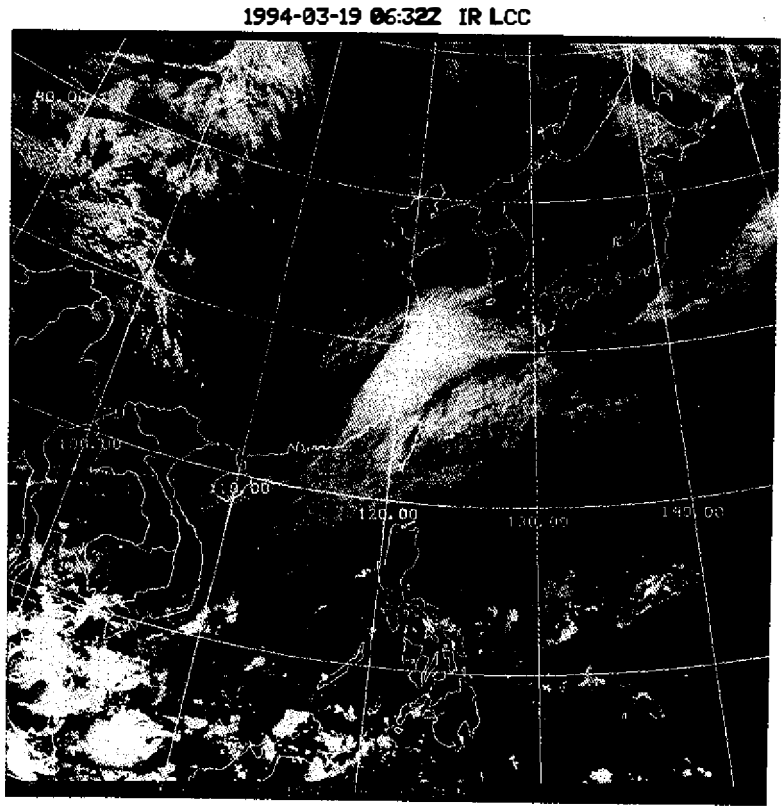


*Fig. 6.* The GMS-4 IR image taken at 0632 GMT (local standard time 14:32), March 19, 1994.

where $L$ is the height of the rain layer, $\gamma_r = a(f)R^{b(f)}$ is the specific attenuation coefficient, $R$ is the rain rate in mm/h, and $a$ and $b$ are constants that depend on frequency, temperature and the size distribution of droplets. At $f\gamma$ = 13 GHz and a rain temperature of 20°C, $a$ = 0.023 and $b$ = 1.18 for Laws and Parsons' droplet size distribution (Olsen *et al.*, 1978; Ippolito, 1986). To use the above formula for rain estimates, it is necessary to give both $Q$ and $L$.

The maximum values of $\Delta T_B$ for the subsequent peaks ranged between 40°K and 100°K (Figure 5). The second largest $\Delta T_B$ maximum ($\Delta T_B$ = 125°K) with a shorter duration (about 6 min for the main peak) was observed at 0515 LST on March 20. The $\Delta T_B$ values reached 40-60°K between 0100 and 0200 LST on March 20 too. The Rain rate and contribution of rain to the atmospheric emission were significantly lower than that during the time of the largest maximum increments in $\Delta T_B$. The increased values of $\Delta T_B$ lasted about 20-40 minutes (and even less time if the fine structure of the $T_B$ variations are taken into account - see Figure 5). Assuming that the wind speed at the cloud level was 10 m/s, an average horizontal size of rain cells of about 7 to 15 km was obtained.

A comparison of the brightness temperature variations with the Keelung rain gauge records demonstrates that they are in good agreement. A rain gauge records the level of collected rain water (in millimeters) as a function of time (Figure 7). The rain rate for a

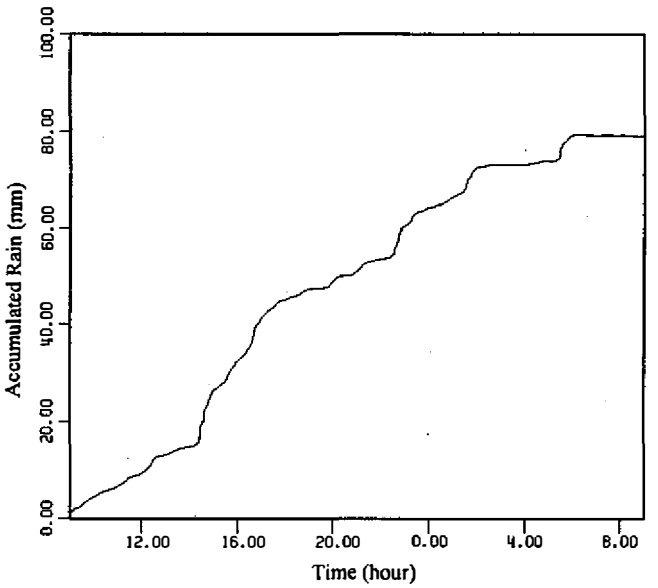


*Fig. 7.* The integrated rain fall over the Keelung weather station between 0900 LST on March 19 and 0900 LST on March 20, 1994. The periods of heavy rains correlate well with the peaks of the brightness temperature increments in Figure 5.

given interval is equal to the change in the rain water level during that time interval. On March 19 and 20, the highest rain intensities for 10-min and for 1-h intervals were 5 mm and 14 mm respectively. Both these intervals began as of 1424 LST on March 19. During this period, the $\Delta T_B$ reached its maximum (Figure 5). The smallest increments of the rain gauge level (less than 1 mm) coincided with time intervals of 0230-0500 LST and after 0550 LST on March 20 when low $\Delta T_B$ values were observed (Figure 5). A tight relation closeness of microwave and rain gauge data is more obvious if the latter (Figure 7) is compared with the integrated increment in the brightness temperature as a function of time (Figure 8) derived from Figure 5. The discrepancies between the two curves are relatively small and they can be well explained if the different nature of the two techniques is considered. The variations in the brightness temperatures are caused by both the rain and the total liquid water content changes inside of a definite volume (see Figure 3a) inside the view of microwave radiometer, while the rain gauge data are point measurements of the rain only. The distance between the microwave radiometer and the rain gauge sometimes could be relatively large in comparison with sizes of rain cells. (The second factor has a more serious influence on the level of correlation for convective rains where the typical sizes of the rain cells are less than those for strati-form rains).

## 6. CLOUD ABSORPTION AT SSM/I FREQUENCIES

The influence of water clouds on the microwave observations of the ocean increases with frequency. Figure 9 depicts a set of normalized curves of $\Gamma_{cl}(f)$ relative to $\Gamma_{cl}$ at $f_o$ = 13.1 GHz. Calculations were performed for the SSM/I frequencies on the assumption that an inequality of $a\lambda \leq 0.2$ holds for all wavelengths including $\lambda \approx 3.5$ mm ($f$ = 85.5 GHz).

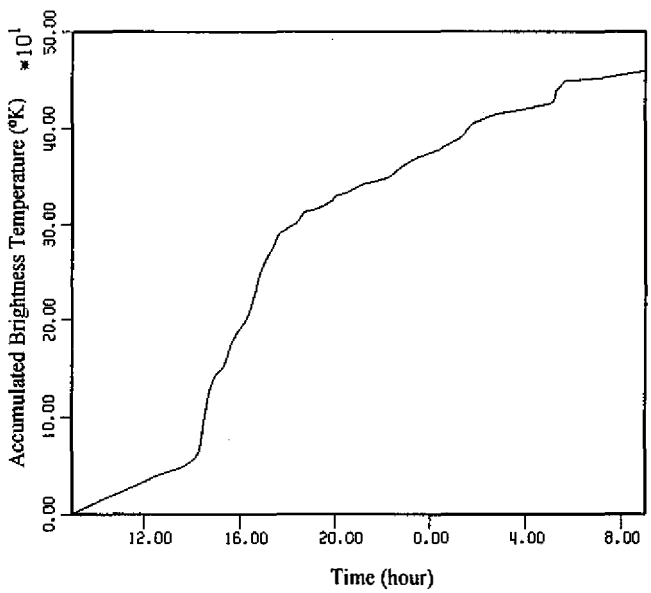


*Fig. 8.* The integrated increment of the brightness temperature of the cloudy atmosphere at wavelength of 2.3 cm in Keelung on March 19-20, 1994.

As seen from Figure 9, the ratio of cloud absorptions changes significantly with temperature. The cloud absorption at $f$ = 85.5 GHz is larger than that at $f_o$ = 13.1 GHz by a factor of 6.3 to 37.3. At lower frequencies, the dependency on $t_{cl}$ is minor, being between 1.88 and 2.17 for $f$ = 19.35 GHz. But at $f$ = 37 GHz, this ratio rises to 4 to 7.8. These features and the errors from calculating the cloud absorption are completely determined by the spectrum of dielectric permittivity of water and the ambiguities in $\varepsilon'$ and $\varepsilon''$ (Mitnik, 1979, 1984). The ambiguities increase with frequency and with the decrease in the value of $t_{cl}$ (Mitnik, 1984; Liebe, 1991).

## 7. DISCUSSION AND CONCLUSIONS

From the above, it follows that any microwave sensing of the ocean from ships, aircrafts or satellites must take cloud absorption and emission into account. This is necessary both for millimeter and centimeter wavelengths. As an illustration, consider the change in the brightness temperature over the ocean for satellite sounding at vertical ($v$) and horizontal ($h$) polarizations, $\Delta T_B^{v,h}(f)$, caused by an appearance of cloudiness. Near the Taiwan area, typical values during the winter monsoon are: $Q$ = 0.3 kg/m$^2$, $t_{cl}$ = 10°C, $V$ = 40-50 kg/m$^2$, sea surface temperature 22°C~25°C, salinity 35‰ and wind speed 5~15 m/s. The theoretical values of the cloud-induced increments in the brightness temperature relative to the $T_B^o$ values over the cloudless ocean were calculated according to the microwave radiative transfer models (Mitnik, 1987; Petty and Katsaros, 1992, 1994). The total cloud absorption is represented by $\Gamma_{cl}(\beta) = \gamma_{cl} \times Q \times \sec\beta$. For $f$ = 13 GHz, at the incidence angle of $\beta$ = 53°(as for the SSM/I), $\Gamma_{cl}(53°)$ is equal to 0.0271×0.3×1.662 = 0.0135 (see Table 3), $\Delta T_B^h \approx$ 5.0°K and $\Delta T_B^v \approx$ 2.9°K. These increments increase with frequency due to the increase in cloud absorption (see Figure 2 and Figure 9). For instance, at $f$ = 37.0 GHz, $\Gamma_{cl}(53°)$ = 0.2047×0.3×1.662 = 0.102, $\Delta T_B^h \approx$ 22.5°K and $\Delta T_B^v \approx$ 11.2°K.

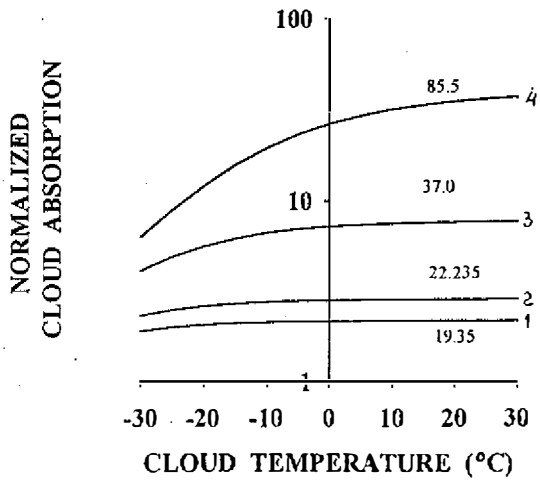


*Fig. 9.* The dependencies of cloud absorption at the SSM/I frequencies on cloud droplet temperature normalized relative to $f_o$ = 13.1 GHz: (1) $f$ = 19.35 GHz, (2) $f$ = 22.23 GHz, (3) $f$ = 37.0 GHz, and (4) $f$ = 85.5 GHz.

The above model calculations and satellite data confirm that the retrieval of oceanic and atmospheric parameters from multichannel microwave measurements do not cause fundamental difficulties in cases with strati-forms clouds characterizing relatively small values of $Q$ at smooth spatial variations. Such conditions were observed at more than 80% of all cloud situations. An analysis of the measurements in this study showed that the clouds and rains with a large liquid water content have relatively short durations and, therefore, a small size. For instance, during the period between March 14 and 26, 1994, clouds with $Q \geq 1.0$ kg/m$^2$ were observed 2.5% of the total time (see Table 4). More detailed Close estimates may be obtained from the statistics of the long term attenuation data on earth-space paths obtained in the regions with similar climatic characteristics (Ippolito, 1986).

Table 4. Relative occurrence of total cloud liquid water content.

| Total liquid water content, (kg/m$^2$) | $0 \leq Q < 0.3$ | $0.3 \leq Q < 0.5$ | $0.5 \leq Q < 1.0$ | $\geq 1.0$ |
|---|---|---|---|---|
| Relative duration, (%) | 81 | 12.3 | 4.2 | 2.5 |

From the above, it follows that the results of ocean parameters retrieved by microwaves are disturbed relatively rarely. Since the characteristics of the ocean has a longer time scale in comparison with the atmospheric ones, a microwave data set which has a short-term interruption causes smaller problem in analyzing oceanic processes than a satellite IR sensing data set which often has long-term interruptions due to the atmospheric interference. The regions with large atmospheric attenuation due to heavy clouds and rain can be distinguished and discarded for further analysis. For example, the difference in the brightness temperatures at vertical and horizontal polarizations at 37 GHz frequency is used to solve this problem (Goodberlet and Swift, 1992; Wentz, 1992).

The isolated rain cells of small sizes occupy only part of the field of view of the SSM/I (Hollinger, 1989) and the other satellite microwave radiometers; thus, their detection presents serious difficulties. One possible approach to overcome this problem off Taiwan coast is to use ground meteorological radars located in Kaohsiung and Hualien. Digital radar reflectivity data allow for the mapping of the spatial distribution of heavy clouds and precipitation at 4 km resolution (Petty and Katsaros, 1991; Chang *et al.*, 1993). The joint analysis of satellite microwave and ground radar data is a new perspective on and direction in the research on both atmospheric and oceanic phenomena.

**Acknowledgements** This research was supported by the National Science Council under grants NSC-83-0102-C019-004-SM, NSC-84-2611-M-019-009, NSC-83-0209-M019-010, NSC-83-0209-M002a-030Y and the Council of Agriculture under research grants 83-RS-04-02 and 84-RS-02. The authors wish to thank Mr. Kuang-Hwa Wang at the Meteorological Satellite Center of the Central Weather Bureau for supplying the radiosonde data and GMS images, and Director Lee at the Keelung Weather Station for supplying the rain gauge data. The authors also thank two anonymous reviewers for their valuable comments.

## REFERENCES

Bauer, P., and P. Schluessel, 1993: Rainfall, total water, ice water, and water vapor over sea from polarized microwave simulations and Special Sensor Microwave/Imager data. *J. Geophys. Res.*, **98**, 20,737-20,759.

Brown, R. A., and G. Levy, 1986: Ocean surface pressure fields from satellite sensed winds. *Mon. Wea. Rev.*, **114**, 2197-2206.

Chang, A. T. C., L. S. Chiu, T. C. C Wang, P. L. Lin, and G. R. Liu, 1993: A preliminary analysis of the Taiwan Hualien radar data. *TAO*, **4**, 17-33.

Central Weather Bureau, 1991: Climatic Atlas of Taiwan, Republic of China, Vol. II. B.-C. Lee (Chief Editor), CWB, Ministry of Communication, ROC. 128pp.

Chernyak, M. M., 1970: Attenuation of electromagnetic radiation by small water droplets. *Trudi VGI*, **17**, 274-276 (in Russian).

Deirmendjian, D., 1975: Far infrared and submillimeter wave attenuation by clouds and rain. *J. Appl. Meteor.*, **14**, 1584-1593.

Demoz, B. B., A. W. Huggins, J. A. Warburton, and R. L. Smith, 1993: Field performance of a spinning-reflector microwave radiometer. *J. Atmos. Oceanic Tech.*, **10**, 420-427.

Grankov, A. G., 1992: Microwave radiometric diagnostics of integral fluxes of sensible heat at the ocean-atmosphere boundary. *Izvestiya, Atmos. Oceanic Physics*, **28**, 883-889.

Goodberlet, M. A., and C. T. Swift, 1992: Improved retrievals from the DMSP wind speed algorithm under adverse weather conditions. *IEEE Trans. Geosci. Remote Sens.*, **30**, 1076-1077.

Hollinger, J. P., 1989: DMSP Special Sensor Microwave/Imager calibration/validation, NRL Final. Report Volume 1., Naval Research Laboratory, Washington, DC., 176pp.

Ippolito, L. J. Jr., 1986: Radiowave Propagation in Satellite Communications. Van Nostrand Reinhold Company, New York, 241pp.

Kummerov, C., and J. A. Weinman, 1988: Determining microwave brightness temperatures from precipitating horizontally finite and vertically structured clouds. *J. Geophys. Res.*, **93**, 3720-3728.

Liebe, H. J., G. A. Hufford, and T. Manabe, 1991: A model for the complex permittivity of water at frequencies below 1 THz. *Int. J. IR Millimeter Waves*, **12**, 659-675.

Liu, W. T., 1986: Statistical relation between monthly mean precipitable water and surface-level humidity over global oceans. *Mon. Wea. Rev.*, **14**, 1591-1602.

Liu, W. T., 1988: Moisture and latent heat-flux variabilities in the tropical Pacific derived from satellite data. *J. Geophys. Res.*, **93**, 6749-6760.

Mitnik, L. M., 1979: Investigation of cloudiness by the microwave radiometric method. VNIIGMI-MCD, Obninsk, 72pp (in Russian).

Mitnik, L. M., 1984: Dielectric permittivity of water: Necessity of accurate values for solving problems of remote sensing of the environment. *Issledovanie Zemli iz Kosmosa (Soviet J. Remote Sensing)*, **3**, 66-71 (in Russian).

Mitnik, L. M., 1986: Microwave radiometric investigation of cloud characteristics from satellite. *Acta Astronautica*, **13**, 175-184.

Mitnik, M. L. 1987: Calculation of spectra of inherent radio thermal radiation of the atmosphere-underlying surface system. Preprint. Pacific Oceanological Institute, Far Eastern Scientific Center, USSR Academy of Sciences, Vladivostok, 32pp (in Russian).

Olsen, R. L., D. V. Rodgers, and D. B. Hodge, 1978: The relation in the calculation of rain attenuation. *IEEE Trans. Ant. Propag.*, **AP-26**, 318-329.

Pacific Ocean. Atlas, 1974: Ministerstvo oboroni SSSR. Voenno-Morskoi Flot (in Russian).

Petty, G. W., and K. B. Katsaros, 1992: The response of the SSM/I to the marine environment. Part I: An analytic model for atmospheric component of observed brightness temperatures. *J. Atmos. Oceanic Tech.*, **9**, 746-761.

Petty, G. W., and K. B. Katsaros, 1992: Nimbus 7 SMMR precipitation observations calibrated against surface radar during TAMEX. *J. Appl. Meteor.*, **31**, 489-505.

Platt, C. M. R., 1970: Transmission of submillimetre waves through water clouds and fogs. *J. Atmos. Sci.*, **27**, 421-425.

Pruppacher, H. R., 1981: The microstructure of atmospheric clouds and precipitation. In: P. V. Hobbs and A. Deepak (Eds.), Clouds: Their Formation, Optical Properties, and Effects. 93-186.

Ray, P. S., 1972: Broadband complex refractive indices of ice and water. *Appl. Optics*, **11**, 1836-1844.

Rosenberg, V. I., 1972: Scattering and attenuation of electromagnetic emission by atmospheric particles, Hydrometeoizdat, Leningrad, 348pp (in Russian).

Schulz, J., P. Schlussel, and H. Grassl, 1993: Water vapour in the atmospheric boundary layer over oceans from SSM/I measurements. *Int. J. Remote Sensing*, **14**, 2773-2789.

Shifrin, K. S., 1951: Scattering of light in a turbid medium. Gostekhizdat. 288pp (in Russian).

Shifrin, K. S., and M. M. Chernyak, 1974: Thermal emission of water droplets in the microwave range. Izvestiya AN SSSR, *Physika atmospheri i okeana*, **10**, 1107-1110 (in Russian).

Van de Hulst, C. H., 1957: Light Scattering by Small Particles, Wiley and Sons, 470pp.

Wentz, F. J., 1992: Measurement of oceanic wind vector using satellite microwave radiometers. *IEEE Trans. Geosci. Remote Sensing*, **30**, 960-972.